Processability and tensile performance of continuous glass fiber/polyamide laminates for structural load-bearing applications

Nikforooz, M[1,3], Golzar, M[1*], Shokrieh, MM[2], Montesano, J[3]

[1] Department of Mechanical Engineering, Tarbiat Modares University, Jalaale-al Ahmad Ave., P.O. Box 14115-143, Tehran, Iran
[2] Composite Research Laboratory, Center of Excellence in Experimental Solid Mechanics and Dynamics, School of Mechanical Engineering, Iran University of Science and Technology (IUST), Narmak, 16846-13114 Tehran, Iran
[3] Department of Mechanical & Mechatronics Engineering, University of Waterloo, 200 University Ave. West, Waterloo, Canada N2L3G1
* Corresponding author (m.golzar@modares.ac.ir; Tel. +98-21-82884320)

Abstract

The performance of continuous E-glass/polyamide 6 laminates processed using distinct hot press moulding cycles was assessed and compared with similar E-glass/epoxy and E-glass/polypropylene laminates. The effects of peak processing temperature, preheating time, and temperature dwell time on laminate consolidation and quality were observed using optical and scanning electron microscopy. Corresponding quasi-static tensile tests were performed on $[0]_8$, $[90]_8$, $[0_2/90_2]_s$ and $[\pm45]_{2s}$ laminates. Compared to E-glass/epoxy composites, the $[0]_8$ specimens presented a similar strength, while the $[90]_8$ specimens exhibited a much lower strength due to weaker fiber/matrix adhesion. Conversely, the E-glass/polyamide cross-ply laminates had a markedly higher strength while exhibiting the same modulus. This is because of higher toughness; the polyamide matrix provides as was proved by higher transverse matrix cracking strain of E-glass/polyamide. These findings support the feasibility of producing cost-effective and high-quality E-glass/polyamide laminates for use in high-performance applications, which is an attractive alternative to more conventional glass/epoxy laminates.

Keywords: A. Polymer-matrix composites (PMCs); A. Thermoplastic resin; B. Mechanical properties; D. Mechanical testing; E. Compression moulding

1 Introduction

Thermoplastic composite materials are attracting major interest in different industry sectors due to their many advantages when compared to thermosetting based composites, including the high ductility and toughness, good chemical resistance characteristics, recyclability, as well as the weldability.

However, their use in high volume production applications is limited due to some key challenges. For example, some thermoplastics, including polyamide, are readily oxidized when heated above their melting temperature. Also, the ability to control fiber alignment during processing is challenging due to high shear forces imparted by the highly viscous matrix. Glass and carbon fibers are commonly used to reinforce thermoplastic polymers such as polyamide, polypropylene and PEEK. These materials can be categorized according to the length of the reinforcing fibers: short and long fiber reinforced composites (SFC, LFC) and continuous fiber reinforced composites (CFC). Many studies [1-3] focused on the processing, mechanical characterization and damage monitoring of short and long fiber thermoplastic composites, demonstrating clear performance improvements with increasing the fiber length [4].

The CFCs are known to have superior mechanical properties and also retention of strength and modulus in different environmental conditions when compared to their SFC and LFC counterparts [5]. However, the volume of the published works on processing and characterization of continuous fiber thermoplastic composites is limited to high performance composites such as carbon/PEEK, which are frequently processed by compression moulding. Jar et al. [6] studied the effect of peak processing temperature on the tensile strength of compression moulded carbon/PEEK specimens, where it was concluded that increasing this temperature by 20°C would increase the composite tensile strength. Fujihara et al. [7] included the effect of holding time apart from the peak processing temperature on the bending strength of unidirectional carbon/PEEK composites. It was concluded that temperatures higher than 380 °C and holding times higher than 10 minutes resulted in a degradation of matrix material and therefore reduced the bending strength of the composite. The cooling rate was also found to have a large effect on fiber/matrix interfacial strength in carbon/PEEK composites [8], whereby increasing the cooling rate enhanced the interfacial strength due to a higher degree of matrix crystallinity around fibers.

Compared to PEEK, polyamides are also known to have excellent stiffness and strength and high toughness [9,10], while substantially more cost effective and requiring drastically lower processing temperatures since they can be polymerized in situ [11]. When they are reinforced with continuous

glass or carbon fibers it is anticipated that their mechanical properties will be comparable to high performance thermoplastic composites. However, prior to integrating continuous glass or carbon fiber/polyamide composites into structural components, their characteristics and mechanical performance under different loading conditions [12,13] and different environmental conditions [14] must be assessed and processing challenges should also be addressed. Currently glass/epoxy composites are widely used for manufacturing wind turbine blades and automotive parts, thus, in order to substitute glass/epoxy with glass/polyamide, the mechanical properties of corresponding laminates should be compared in a similar fashion as has been conducted for carbon/polyamide and carbon epoxy composites [15,16].

Some reported studies have focused on the mechanical behavior of continuous glass fiber/polyamide composites, particularly in shear and flexural loadings. Cinquin et al. [17] studied the effect of different additives on the performance of unidirectional glass/polyamide composites. The significant effect of thermal stabilizers in improving the dynamic shear modulus and flexural fatigue strength of glass/polyamide composites was identified. Yan et al. [18] investigated the flexural and shear strengths of vacuum infusion moulded glass/polyamide composites. They investigated the content of catalyst and processing temperature on the degree of crystallinity and strength of the produced composite. Cartledge and Baillie [19] studied the effect of cooling rate on the Iosipescu shear strength and transverse flexural strength of glass/polyamide composites. They concluded that lowering the cooling rate enhanced the interfacial tensile and shear strengths through improving the crystallinity of the polyamide and also the transcrystallinity between glass fibers and polyamide. Von Rijswijk [11] studied the processing of woven glass fiber reinforced polyamide via the resin transfer moulding of anionic polyamide-6 (APA-6). The mould temperature was optimized for maximizing the interfacial shear and fatigue strengths of the material, which were compared with those of glass/epoxy composites. Probhakaran et al. [20] examined the compression, bending and short beam shear behaviors of glass fiber reinforced polyamides with three different commercial prepregs and comingles. Generally, the laminate produced from comingles showed improved mechanical properties due to the proper alignment of fibers, even distribution and improved wetting of the fibers with the

matrix. Haspel et al. [21] characterized the shear strength of glass/polyamide and glass/epoxy composites produced by resin transfer moulding using a push out test. It was concluded that glass/epoxy composite had a very high interfacial shear strength compared to glass/polyamide composites.

A review of the literature indicates that there is limited research focused on assessing the performance of multidirectional glass/polyamide laminates and that the knowledgebase for polyamide-based continuous fiber-reinforced composites has not yet reached an acceptable level of maturity, which would otherwise be valuable for the design and manufacturing of corresponding composite structures such as wind turbine blades and automobile bumper beams. The initial goal of this study was to investigate the influence of processing parameters on the in-plane tensile performance of unidirectional and cross-ply E-glass/polyamide laminates. The consolidation and processing qualities for laminates fabricated by the two main compression moulding process cycles were investigated using optical and scanning electron microscopy (SEM). Furthermore, the performance of these laminates under quasi-static in-plane tensile loading was studied and compared to that of the E-glass/epoxy and E-glass/polypropylene composites with similar fiber volume fractions. This study represents an initial step towards integrating high quality cost effective E-glass/polyamide composites into primary load-bearing structures by replacing conventional E-glass/epoxy laminates.

2 Material and processing

2.1 Materials

Unidirectional E-glass/polyamide 6 tape supplied by Jonam Composites Ltd. was used for producing composite laminates. Prior to processing, the nominal volume fraction and the total areal weight of the prepregs were 45% and 370 g/m^2, respectively. Moreover, the width and thickness of the tape were 110 mm and 0.2 mm, respectively.

2.2 Processing

Two processes were used for fabricating 110 x 110 mm composite laminate plates as will be described in this section. Picture frame moulds were prepared from 6061 aluminum alloy as shown in

Fig. 1, and used for both processes. The prepregs were stacked according to the specified lamination in the mould cavity between the walls, and the walls were bolted down to the lower mould plate. Teflon sheets were used on the top and bottom of the laminate to prevent the adhering of laminate to the mould; and a caul plate was used at the top of the prepregs as shown.

The first group of laminates was processed using a manual hot press machine as shown in Fig. 2(a). The platens were pre-heated to 255 °C, then the mould was placed between the platens and the pressure-temperature cycle shown in Fig. 2(b) was applied. Cooling of the platens was accomplished by water such that the mean cooling rate was 10 °C/min. This will hereafter be denoted as process-A. To limit the oxidation observed along the panel edges which permeated through to the middle of the panels with the manual hot press, some key modifications were made to the procedure. First, an automatic 30-ton Carver hot press with a notably higher heating capacity was used (see Fig. 3(a)), allowing the mould to reach the maximum temperature four times faster than the manual hot press. Subsequently, the process was systematically optimized by varying the peak processing temperature and the temperature dwell time. It should be noted that the mean cooling rate was held constant at 10 °C/min. A summary of the optimization process is presented in the subsequent paragraph.

In order to optimize the process, the peak processing temperature was varied to reduce the time at which the laminate is exposed to temperatures higher than the melting point of polyamide (T_m = 220 °C). In Fig. 4 the oxidation induced along the edges of the panels is illustrated for three different maximum temperatures and dwell times: 215 °C and 225 °C with 7-minute dwell time and 240 °C without dwell time. For the first condition, the peak processing temperature was 5 °C below the melting temperature and oxidation was vast due to the lack of consolidation in the panel edges and existence of air between the layers. Similarly, for the second peak processing temperature of 225 °C, the consolidation was not optimal and there was still notable oxidation on the edges as shown in Fig. 5. When the temperature was increased to 240 °C, which is 20 °C higher than the melting temperature of the prepreg, and the dwell time removed, the observed oxidation was minimal and confined to small region near the panel edges (see Fig. 4). Once the processing temperature was increased beyond 250 °C with or without any dwell time, the degree of oxidation increased. In the optimized

temperature-time cycle, the time at which samples were exposed to temperatures higher than the prepreg melting temperature was reduced to 2-3 minutes to ensure a reduction in oxidation reaction time. Temperature-time and pressure-time cycle of this process, hereafter denoted as process-B, is shown in Fig. 3(b).

2.3 Optical Microscopy

Optical microscopy was used on the laminates produced using both process-A and process-B to investigate the impregnation of the glass fibers. As seen in Fig. 5, the quality of the impregnation is noticeably high. It should be noted that some voids and resin rich areas have been observed in both types of specimens as is shown in the figure. Qualitative observations have confirmed that the void content is similar for laminates produces using both process-A and B.

The optical images were also used in ImageJ software to compute the volume fraction of the specimens. The obtained volume fraction for all specimens was approximately 58 %.

3 Mechanical testing results and discussion

Tensile static tests were performed on $[0]_8$, $[90]_8$, $[0_2/90_2]_s$, $[0_4/90_4]_s$ and $[\pm45]_{2s}$ specimens in accordance with ASTM D3039. For this purpose, an MTS 810 hydraulic test frame was used for the $[0]_8$ and $[90]_8$ laminations, and for the remaining laminations an Instron 8874 hydraulic test frame was used. The displacement rate was set at 2 mm/min for all tests. Strain was measured by a 10 mm gauge extensometer, while digital image correlation (DIC) was also used for a number of the test specimens. At least five specimens were tested for each lamination, and the mean value was reported for both strength and Young's Modulus. Aluminum end tabs of 2 mm by 2 mm size were bonded to both ends of all specimens. Fig. 6 and Table 1 summarize the dimensions of the different test specimens used in this study.

After completion of the tensile static tests, some of the fractured specimens were gold coated using a Polaron Instruments E5100 SEM Coating System and LEO (Zeiss) 1550 and Philips XL30 microscopes were used to observe the morphology of fractured surfaces.

3.1 $[0]_8$ laminates quasi-static tension tests

The representative stress-strain curves for E-glass/polyamide $[0]_8$ laminates fabricated using process-A and B are presented in Fig. 7, which follow a linear profile as shown. The mean strength and Young's modulus of the process-A samples are respectively 835±69.5 MPa and 42.1±1.6 GPa. The mean strength and the Young's modulus for the process-B specimens are 885±78.5 MPa and 41.6±3.7 GPa, respectively, which are comparable to the process-A specimens. The stress-strain curves of the process-A samples exhibited a sudden drop near 2% strain with subsequent rise (see Fig. 7). This behavior may be due to the onset of notable splitting crack formation prior to specimen failure, which can be attributed to the reduced mechanical properties of polyamide caused by oxidation and thus a lower fiber/matrix interfacial strength. This is confirmed through SEM images in the following section. It should be noted that the failure strain for each glass/polyamide specimen was approximately 2.5%.

For obtaining the Poisson's ratio, the DIC was used for some of the tested samples. After analyzing the strain fields and according to the definition of $\nu_{12} = -\varepsilon_2 / \varepsilon_1$, the measured Poisson's ratio was equal to 0.28. The Poisson's ratio value obtained using the rule of mixtures expressions with a 58% fiber volume fraction was 0.29, which is comparable. Similarly, the theoretical longitudinal Young's modulus for the E-glass/polyamide material is 43.39 GPa, which is also very close to the measured experimental value for the process-A and B specimens. This suggests that the resulting void content and any process-induced fiber misalignment is considered to be low, which supports the high quality of the E-glass/polyamide specimens.

The experimental stress-strain curves for the E-glass/polyamide $[0]_8$ specimens were also compared with those of E-glass/epoxy and E-glass/polypropylene with maleic anhydride (MA) having the same fiber content. As shown in the Fig. 7 and Table 2, the longitudinal Young's modulus of both glass/polyamide specimens are approximately the same as glass/epoxy, however, the strength of the glass/polyamide specimens is slightly lower than glass/epoxy. Nonetheless, under fiber-dominated loading conditions the performance of the glass/polyamide specimens is comparable to that of glass/epoxy. The longitudinal Young's modulus of glass/polyamide is also comparable to that of

glass/polypropylene (with and without MA) which is expected since polypropylene and polyamide have comparable Young's moduli. Also, the strength of glass/polyamide is similar to glass/polypropylene with 10 % wt. MA, which is attributed to the improved fiber/matrix interfacial strength of the glass/polypropylene due to the added MA.

3.1.1 Scanning Electron Microscopy (SEM) of $[0]_8$ laminates

Images of tested $[0]_8$ specimens are shown in Fig. 8(a) reveal the presence of many longitudinal splitting cracks. SEM images perpendicular to the splitting crack surfaces for two $[0]_8$ laminates fabricated with process-A and process-B are shown in Fig. 8(b). For both processing conditions, cracks initiated in the matrix or at the interface between fiber and matrix (see Fig. 8(b)), and propagated along the fiber direction until they formed into long splitting cracks. The sequences of splitting type failures occurred in different sites of the specimen as was shown in Fig. 8(b), which was followed by fiber fracture and finally resulting in failure of the specimen. It should be mentioned that fiber fracture was very localized in a small zone, which has been also observed in ref. [20]. As illustrated in Fig. 8(b), process-A specimens had a significant number of bare fibers at the fracture surface in comparison to the process-B specimens. This is indicative of fiber/matrix debonding, confirming lower fiber/matrix interface strength for the process-A specimens. This was likely caused by the degradation of matrix resulting from oxidation [25], which promoted poor adhesion between the fibers and matrix.

3.2 $[90]_8$ laminates quasi-static tension tests

The representative stress-strain curves for $[90]_8$ laminates of E-glass/polyamide fabricated with process-A and process-B, E-glass/epoxy (50% fiber volume content) with different sizings, and E-glass/polypropylene with 10 wt. % and 40 wt. % of MA and without MA are shown in Fig. 9. The mean transverse strength increased by nearly 35% and the mean Young modulus increased by 15% from process-A to process-B (see Table 3), which again suggests that the optimized process results in superior fiber/matrix interfacial strength. The failure strains for both glass/polyamide specimens are between 0.35% and 0.4%, which approximately corresponds to the matrix failure strain of 0.3%. The

transverse modulus evaluated with the rule of mixtures expression results in a value of E_2 = 5.69 GPa, which is comparable to the measured value of the specimens fabricated with process-B. This further supports the improved quality of the process-B specimens.

From Fig. 9 and Table 3, the strength of $[90]_8$ glass/epoxy laminates is at least 2.5 times more than that of $[90]_8$ glass/polyamide, with a notably greater modulus. The decreased performance of the glass/polyamide specimens in the matrix-dominated transverse direction when compared to glass/epoxy may be a result of relatively weaker bonding between the glass fibers and polyamide [18]. Furthermore, the strength of the $[90]_8$ glass/polypropylene specimens is lower than that of the glass/polyamide samples tested here, however, by adding 10 % wt. MA the glass/polypropylene has the same transverse strength as glass/polyamide.

3.2.1 Scanning Electron Microscopy (SEM) of $[90]_8$ laminates

Failed $[90]_8$ E-glass/polyamide test specimens are shown in Fig. 10(a). The fracture surfaces were fairly localized and brittle in nature at the macroscopic length scale, consisting of a single crack across the specimen width. The corresponding fracture surfaces are shown in Fig. 10(b). For the samples which were fabricated using process-A, many bare fibers and debonding between fiber and matrix are observed. For the samples which were fabricated by process-B, debonding occurred in some regions of the fiber surface, while for the majority of fibers significantly improved fiber/matrix adhesion was observed. Many localized matrix hackles on the fiber surfaces illustrate the strength of the fiber/matrix interface (see Fig. 10(b)). These results further support the fact that process-B results in lower matrix degradation and improved fiber/matrix interfacial strength.

3.3 $[0_n/90_n]_s$ cross-ply laminates quasi-static tension tests

The representative stress-strain curves and corresponding mechanical properties for $[0_2/90_2]_s$ and $[0_4/90_4]_s$ laminates fabricated with process-B, $[0_2/90_2]_s$ laminates fabricated with process-A, and a $[0_2/90_2]_s$ glass/epoxy laminate are presented in Fig. 11 and Table 4. The mean strength and Young's modulus of $[0_2/90_2]_s$ glass/polyamide laminates increased by 24.4 % and 26.7 %, respectively, which further confirms the improved fiber/matrix adhesion and interfacial strength for process-B specimens.

This result is not surprising when considering the improved transverse properties of the process-B $[90]_8$ glass/polyamide specimens, which suggests that the 90° layers for the process-B cross-ply laminates exhibit micro-cracking at higher loads, and thus fail at a higher stress level when compared to the equivalent process-A cross-ply laminates.

Fig. 11 and Table 4 also show that the Young's modulus of glass/epoxy and glass/polyamide are comparable for the $[0_2/90_2]_s$ lamination; however, the strength of glass/epoxy is nearly 16% lower than that of glass/polyamide. This is due to the fact that transverse cracks in the glass/epoxy initiate at very low applied strain (0.25%), which notably decreases the Young modulus.

To further investigate the initiation and propagation of cracks in transverse layers for the process-B E-glass/polyamide $[0_2/90_2]_s$ laminates, the edges of the sample were polished with 6 different grades of sand paper and also with four different grades of alumina polishing suspension. The tensile tests were interrupted at 5 different strains, including 0.25 %, 0.5 %, 0.75 %, 1.0 % and 1.25 %, and the edges were observed under an optical microscope. As seen in Fig. 12 there was no cracking up to 0.5 % strain, and not until 0.75 % strain were cracks observed locally. At 1.0% and 1.25% strains, additional cracks initiated and propagated in different sites of the transverse layer. Compared to the $[0_2/90_2]_s$ glass/epoxy, micro-crack initiation was delayed for the $[0_2/90_2]_s$ glass/polyamide laminates. This result is particularly interesting when the data presented in Table 3 for $[90]_8$ laminates are considered, recalling that the glass/epoxy had notably higher transverse strength when compared to glass/polyamide. In conjunction with the tougher thermoplastic matrix, the constraining effects on the transverse layers from the 0° layers seems to be playing a notable role in delaying damage initiation in the glass/polyamide laminates. This is an important result which demonstrates the importance of in situ ply strength when assessing the performance of multidirectional laminates, in particular for fiber-reinforced thermoplastics. It should be noted that the glass/epoxy laminates have slightly thicker transverse layers when compared to the glass/polyamide laminates, which may also be contributing to crack initiation at lower strains for the glass/epoxy laminates. In addition, since the glass/polyamide have notably lower transverse stiffness, the 90° layers will carry less load compared to the 90° layers in the glass/epoxy laminates, which may also contribute to the delay in crack initiation.

3.3.1 Scanning Electron Microscopy (SEM) of $[0_2/90_2]_s$ laminates

Fractured specimens are shown in Fig. 13(a), where the fracture surface is brittle in nature and perpendicular to the load direction. As seen in the SEM images of the fracture surface in Fig. 13(b) for samples fabricated with process-A, in the central transverse layer there is debonding between the fibers and matrix. In the longitudinal layer there are fiber fractures and localized matrix splitting, as well as fiber matrix debonding and fiber pull out. For samples which were fabricated with process-B, in the central transverse layer good bonding between the fibers and matrix were observed which is consistent with the results for the $[0]_8$ and $[90]_8$ laminates.

3.4 $[\pm 45]_{2s}$ laminates quasi-static tension tests

The representative stress-strain curve of E-glass/polyamide is shown in Fig. 14, demonstrating a high degree of nonlinearity prior to specimen failure. According to ASTM D3518, the shear strength is given by $\frac{\sigma_x}{2}$, which is equal to 75±15 MPa. Based on Equation (1) the approximate shear modulus of the $[\pm 45]_{2s}$ E-glass/polyamide laminate is 2.1 GPa, which is similar to the value of 2.5 GPa evaluated using the rule of mixtures. The stress-strain curve of E-glass/polyamide has been compared with that of E-glass/polypropylene for the same lamination, and also with E-glass/epoxy with $[\pm 45]_{3s}$ and $[\pm 45]_{2s}$ lamination with 50% and 54% fiber content, respectively. As seen in Fig. 14 and Table 5, the in-plane shear strength of E-glass/polyamide is about two times higher than that of E-glass/epoxy reported in Ref. [26], 80% of E-glass/epoxy from Ref. [28], and five to six times higher than that of E-glass/polypropylene based on the maximum failure stress. It should be mentioned that a scissoring effect was observed for E-glass/polyamide in which the fibers tended to rotate and align themselves to the loading direction. This effect contributed to increasing the shear modulus and the shear strength of the glass/polyamide specimens. Although the shear properties reported in the literature for E-glass/epoxy reveal a large scatter, the relative shear strength and stiffness of E-glass/polyamide are comparable, if not improved.

$$G_{12} = \frac{E_x}{2(1-\upsilon_{xy})} \tag{1}$$

4 Conclusions

Continuous E-glass/polyamide composite materials were fabricated by two different process cycles, the first in which the laminate was exposed to the peak processing temperature for 10 minutes (process-A), and the second without a temperature dwell (process-B). For both processing cycles the cooling rate was kept constant at 10 °C/min. It was shown that a faster heating rate along with a reduced peak temperature and reducing holding time at peak temperature notably reduced the observed oxidation in the processed panels. To further investigate the effect of oxidation on mechanical properties of E-glass/polyamide laminates, tensile static mechanical tests were performed on five different laminations including $[0]_8$, $[90]_8$, $[0_2/90_2]_s$, $[0_4/90_4]_s$ and $[\pm45]_{2s}$. The obtained stress-strain curves were also compared to those of E-glass/polypropylene with different percentages of MA, and with that of E-glass/epoxy with different fiber sizings. Static tensile tests showed that glass/polyamide laminates fabricated using process-B generally exhibited superior strength and stiffness when compared to the same laminates fabricated by process-A, particularly for the $[90]_8$ and cross-ply laminates studied. This was attributed to observed oxidation of the polyamide matrix for the process-A specimens, resulting in a reduction in the fiber-matrix interfacial strength. This was confirmed though corresponding SEM micrographs revealing significant fiber/matrix debonding at the fracture surfaces for all process-A laminates studied, which was not observed for the process-B laminates. The exhibited high performance of the process-B E-glass/polyamide laminates provides support for the feasibility of producing high quality thermoplastic-based continuous fiber reinforced composites, which is a significant finding.

Furthermore, the E-glass/polyamide laminates fabricated using process-B exhibited a transverse strength of 18.5 MPa, which is notably lower than the transverse strength of similar E-glass/epoxy laminates, and likely a result of stronger fiber/matrix adhesion for E-glass/epoxy. The longitudinal strength of the E-glass/polyamide was 885 MPa, which is comparable to similar E-glass/epoxy and glass/polypropylene laminates with the same fiber content, demonstrating that the longitudinal strength is mainly affected by the volume fraction of glass fibers and is independent of the type of matrix and different processing conditions. For $[0_2/90_2]_s$ E-glass/polyamide laminates fabricated by

process-B, the Young's modulus was the same as similar E-glass/epoxy laminates with the same fiber content, however, its strength was 19% higher. This important result is attributed to the delayed onset of transverse ply cracking in 90° layers of the E-glass/polyamide cross-ply laminates at an approximate strain of 0.75%, which has mitigated specimen failure until higher stress levels. Note that the reported onset of transverse ply cracking in the E-glass/epoxy cross-ply laminates was at a strain of 0.25%. This notable result may be due to the increased toughness of the polyamide matrix coupled with the specific ply constraining effects for the E-glass/polyamide cross-ply laminate, resulting in a higher in-situ ply strength. This is an important result demonstrating that the in situ constraining effects in E-glass/polyamide laminates is notably greater than those in E-glass/epoxy laminates. These characteristics suggest that glass/polyamide composites may be suitable replacements for glass/epoxy in many high performance applications requiring high strength and damage tolerant structures. Since high quality E-glass/polyamide laminates can be efficiently processed as demonstrated in this study, it would be highly beneficial to integrate glass/polyamide into practical primary structures since these materials can be recycled at the end of their life and also they are drastically inexpensive when compared to high performance thermoplastic and conventional glass/epoxy composites.

Although this study has produced notable results supporting the use of glass/polyamide laminates for high performance applications, additional research is required to improve the knowledgebase for this material system. First, multidirectional glass/polyamide laminates should be studied in order to complement the results presented for cross-ply laminates, which is essential for practical structures requiring specific directional properties. This would provide further understanding of the influence of damage evolution and in situ ply constraining effects for each particular stacking sequence, and provide much needed characterization for development of damage-based simulation models. Also, the fatigue performance of glass/polyamide laminates must be considered for structures in which long-term durability is critical. In particular, understanding the progressive nature of failure and its influence in the mechanical properties under cyclic loading is of key importance for widespread adoption of glass/polyamide material systems. Finally, the performance of E-glass/polyamide

laminates under compressive and bending loads must also be examined to complement this study which was conducted under tensile loading.

Acknowledgements

Tarbiat Modares University and the University of Waterloo are greatly acknowledged for funding in support of the study. The authors would also like to thank Dr. Habiba Bougherara (Ryerson University, Toronto, Canada) for providing access to the infrastructure for processing many of the samples tested.

REFERENCES

[1] Lafranche E, Krawczak P, Ciolczyk J-P, Maugey J. Injection moulding of long glass fiber reinforced polyamide 66: processing conditions/microstructure/flexural properties relationship. Adv Polymer Technol 2005;24(2):114-131.

[2] M. De Monte, E. Moosbrugger, and M. Quaresimin, "Influence of temperature and thickness on the off-axis behaviour of short glass fibre reinforced polyamide 6.6 - Quasi-static loading," *Compos. Part A Appl. Sci. Manuf.*, vol. 41, no. 7, pp. 859–871, 2010.

[3] Rolland H, Saintier N, Wilson P, Merzeau J, Robert G. In situ X-ray tomography investigation on damage mechanisms in short glass fibre reinforced thermoplastics : Effects of fibre orientation and relative humidity. Compos Part B 2017;109:170–86.

[4] Hassan a., Yahya R, Yahaya a. H, Tahir a. RM, Hornsby PR. Tensile, Impact and Fiber Length Properties of Injection-Molded Short and Long Glass Fiber-Reinforced Polyamide 6,6 Composites. J Reinf Plast Compos 2004;23:969–86.

[5] Antoun B. Challenges in Mechanics of Time-Dependent Materials, Volume 2 2015;2:171–5.

[6] Jar PYB, Mulone R, Davies P, Kausch HH. A study of the effect of forming temperature on the mechanical behaviour of carbon-fibre/peek composites. Compos Sci Technol 1993;46:7–19.

[7] Fujihara K, Huang ZM, Ramakrishna S, Hamada H. Influence of processing conditions on bending property of continuous carbon fiber reinforced PEEK composites. Compos Sci Technol 2004;64:2525–34.

[8] Gao SL, Kim JK. Cooling rate influences in carbon fibre/PEEK composites. Part 1. Crystallinity and interface adhesion. Compos Part A Appl Sci Manuf 2000;31:517–30.

[9] Vecchione P, Acierno D, Abbate M, Russo P. Hot-compacted self reinforced polyamide 6 composite laminates. Compos Part B Eng 2017;110:39–45.

[10] Chen JH, Schulz E, Bohse J, Hinrichsen G. Effect of fibre content on the interlaminar fracture toughness of unidirectional glass-fibre/polyamide composite. Compos Part A Appl Sci Manuf 1999;30:747–55.

[11] van Rijswijk K, van Geenen AA, Bersee HEN. Textile fiber-reinforced anionic polyamide-6 composites. Part II: Investigation on interfacial bond formation by short beam shear test. Compos Part A Appl Sci Manuf 2009;40:1033–43.

[12] Botelho EC, Figiel L, Rezende MC, Lauke B. Mechanical behavior of carbon fiber reinforced polyamide composites. Compos Sci Technol 2003;63:1843–55.

[13] Todo M, Takahashi K, Béguelin P, Kausch HH. Strain-rate dependence of the tensile fracture behaviour of woven-cloth reinforced polyamide composites. Compos Sci Technol 2000;60:763–71.

[14] A. Malpot, F. Touchard, and S. Bergamo, "Effect of relative humidity on mechanical properties of a woven thermoplastic composite for automotive application," *Polym. Test.*, vol. 48, pp. 160–168, 2015.
[15] Ma Y, Ueda M, Yokozeki T, Sugahara T, Yang Y, Hamada H. A comparative study of the mechanical properties and failure behavior of carbon fiber/epoxy and carbon fiber/polyamide 6 unidirectional composites. Compos Struct 2017;160:89–99.
[16] Ma Y, Yang Y, Sugahara T, Hamada H. A study on the failure behavior and mechanical properties of unidirectional fiber reinforced thermosetting and thermoplastic composites. Compos Part B Eng 2016;99:162–72.
[17] Cinquin J, Chabert B, Chauchard J, Morel E, Trotignon JP. Characterization of a thermoplastic (polyamide 66) reinforced with unidirectional glass fibres. Matrix additives and fibres surface treatment influence on the mechanical and viscoelastic properties. Composites 1990;21:141–7.
[18] Yan C, Li H, Zhang X, Zhu Y, Fan X, Yu L. Preparation and properties of continuous glass fiber reinforced anionic polyamide-6 thermoplastic composites. Mater Des 2013;46:688–95.
[19] Cartledge HCY, Baillie CA. Studies of microstructural and mechanical properties of Nylon/Glass composite Part I The effect of thermal processing on crystallinity, transcrystallinity and crystal phases. J Mater Sci 1999;34:5099–111.
[20] Prabhakaran RTD, Pillai S, Charca S, Oshkovr SA, Knudsen H, Tom L, et al. Mechanical Characterization and Fractography of Glass Fiber / Polyamide (PA6) Composites 2014:1–20.
[21] Haspel B, Hoffmann C, Elsner P, Weidenmann KA. Characterization of the interfacial shear strength of glass-fiber reinforced polymers made from novel RTM processes. Int J Plast Technol 2015;19:333–46.
[22] Rijsdijk HA, Contant M, Peijs AAJM. Continuous-glass-fibre-reinforced polypropylene composites: I. Influence of maleic-anhydride-modified polypropylene on mechanical properties. Compos Sci Technol 1993;48:161–72.
[23] Carlsson LA, Adams DF, Pipes RB. Experimental characterization of advanced composite materials. CRC press; 2014.
[24] Benzarti K, Cangemi L, Dal Maso F. Transverse properties of unidirectional glass/epoxy composites: Influence of fibre surface treatments. Compos Part A Appl Sci Manuf 2001;32:197–206.
[25] Yang L, Thomason JL. Interface strength in glass fibre-polypropylene measured using the fibre pull-out and microbond methods. Compos Part A Appl Sci Manuf 2010;41:1077–83.
[26] Shokrieh MM, Omidi MJ. Investigation of strain rate effects on in-plane shear properties of glass/epoxy composites. Compos Struct 2009;91:95–102.
[27] Roundi W, El Mahi A, El Gharad A, Rebière J-L. Experimental and numerical investigation of the effects of stacking sequence and stress ratio on fatigue damage of glass/epoxy composites. Compos Part B Eng 2016;109.
[28] Ellyin F, Rohrbacher C. Effect of Aqueous Environment and Temperature on Glass-Fibre Epoxy Resin Composites. Reinf Plast Compos 2000;19:1405–27.

Figures

Figure 1. Picture-frame aluminum alloy hot press mould.

Figure 2. a) Manual hot press machine used in process-A. b) Temperature-time and pressure-time process diagram for fabrication of glass/polyamide used in process-A.

Figure 3. a) 30-ton Carver hot press used in process-B. b) Temperature-time and pressure-time process diagram for fabrication of glass/polyamide used in process-B.

Figure 4. Glass/polyamide laminates fabricated with different processing conditions as specified (blue ovals show the oxidation zones).

Figure 5. Optical microscopy of unidirectional glass/polyamide composite cross-section for a) process-A b) process-B.

Figure 6. Geometry of the specimens used for static tensile tests.

Figure 7. Tensile stress–strain curves for various $[0]_8$ laminates of glass/polyamide, glass/epoxy and glass polypropylene composites.

Figure 8. a) Post-mortem $[0]_8$ glass/polyamide specimens after static tensile test. b) SEM micrographs of fracture surfaces for $[0]_8$ glass/polyamide specimens loaded in the longitudinal direction for specimens fabricated with process-A, and specimens fabricated with process-B.

Figure 9. Tensile stress-strain curves for various $[90]_8$ glass/polyamide, glass/epoxy and glass/polypropylene specimens.

Figure. 10. a) Post mortem $[90]_8$ glass/polyamide specimens after static tensile test b) SEM micrographs of $[90]_8$ glass/polyamide specimen fracture surfaces loaded in the transverse direction for specimens fabricated with process-A, and specimens fabricated with process-B.

Figure 11. Tensile stress-strain curve for $[0_2/90_2]_s$ glass/polyamide and glass/epoxy, and $[0_4/90_4]_s$ glass/polyamide specimens.

Figure 12. a) Post mortem $[0_2/90_2]_s$ glass/polyamide specimens after static tensile test. b) SEM micrographs of fracture surfaces in $[0_2/90_2]_s$ glass/polyamide specimens under quasi-static tensile loading for specimens fabricated with process-A, and specimens fabricated with process-B.

Figure 13. Optical microscopy of the transverse middle layer in $[0_2/90_2]_s$ glass/polyamide laminate illustrating ply crack evolution during quasi-static tensile loading at different applied strains.

Figure 14. Tensile stress-strain curve for angle-ply glass/polyamide, glass/epoxy and glass/polypropylene specimens.

Tables

Table 1

Dimensions of the specimens used for static tensile tests.

Lamination	l_1 **(mm)**	w_1 **(mm)**	w_2 **(mm)**	h_2 **(mm)**	h_1 **(mm)**
$[0]_8$	110	15	20	1.4±0.1	1
$[90]_8$	110	20, 15	20	1.4±0.1	1
$[0_2/90_2]_s$	110	15	20	1.4±0.1	1
$[0_4/90_4]_s$	110	15	20	2.9±0.1	1.5
$[\pm45]_{2s}$	120	12	20	1.4±0.1	1.5

Table 2

Tensile mechanical properties of different composites in the longitudinal direction.

Material	Young's modulus (GPa)	Ultimate strength (MPa)	Volume fraction
glass/polyamide (process-A)	42.1±1.6	835±69.5	0.58
glass/polyamide (process-B)	41.6±3.7	885±78.5	0.58
glass/epoxy [23]	41.8	1034.8	0.6
glass/PP without MA [22]	43.4 ± 1.4	720 ± 50	0.58
glass/PP with 10 wt. % MA [22]	43.6 ± 2.0	890 ±60	0.58

Table 3

Tensile mechanical properties of different composites in transverse direction

Material	Young's modulus (GPa)	Ultimate strength (MPa)	Volume fraction
glass/polyamide (process-A)	4.76±0.3	13.7±2	0.58
glass/polyamide (process-B)	5.47±0.16	18.5±1.5	0.58
glass/epoxy-sizing A [24]	11.5	49.7	0.5
glass/epoxy-sizing C [24]	8.1	57	0.5
Glass/epoxy-no coating [24]	14.9	54	0.5
glass/PP without MA [22]	5.6	8.5	0.58
glass/PP with 10 wt. % MA [22]	6.9	20.5	0.58
glass/PP with 40 wt. % MA [22]	5.8	12.6	0.58

Table 4

Tensile mechanical properties of different composites with $[0_n/90_n]_s$ lamination

Material/Lamination	Young's modulus (GPa)	Ultimate strength (MPa)	Volume fraction
$[0_2/90_2]_s$ glass/polyamide (process-A)	21±0.5	397±57	0.58
$[0_2/90_2]_s$ glass/polyamide (process-B)	26.6±2.5	494.1±32.3	0.58
$[0_4/90_4]_s$ glass/polyamide (process-B)	29.8±2.5	480±28	0.58

$[0_2/90_2]$s glass/epoxy [27]	27	415.6	0.6

Table 5

Tensile mechanical properties of different composites with angle-ply lamination.

Material/Lamination	**Young's modulus (GPa)**	**Ultimate strength (MPa)**	**Volume fraction**
$[\pm 45]_{2s}$ glass/polyamide (process-A)	2.1±0.2	75±15	0.58
$[\pm 45]_{4s}$ glass/PP without MA [22]	not mentioned	9.6 ± 0.8	0.58
$[\pm 45]_{4s}$ glass/PP with 10 wt. % MA [22]	not mentioned	13.6 ± 1.0	0.58
$[\pm 45]_{3s}$ glass/epoxy [26]	4	40	0.5
$[\pm 45]_{2s}$ glass/epoxy [28]	not mentioned	93.3	0.54

Figure(s)

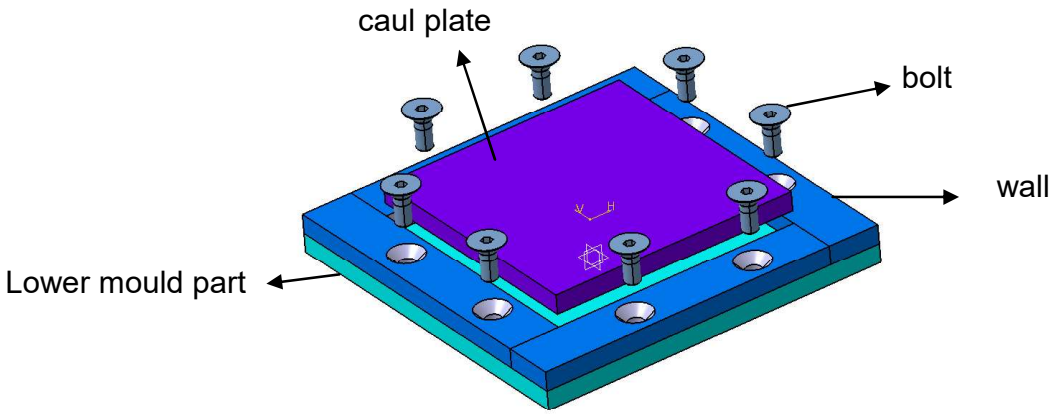

Figure(s)

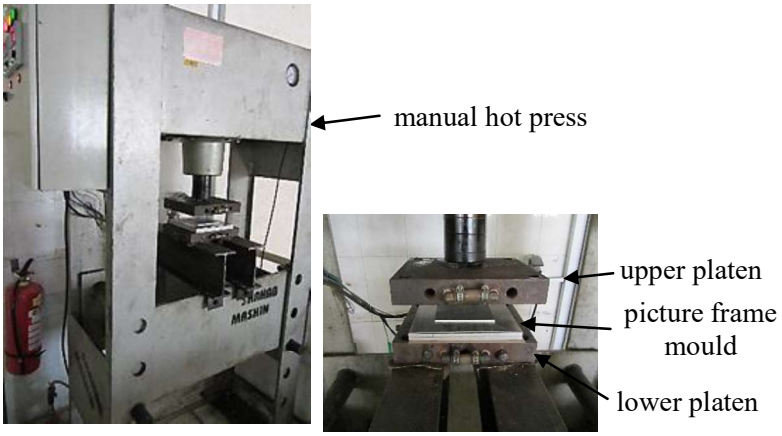
manual hot press
upper platen
picture frame mould
lower platen

(a)

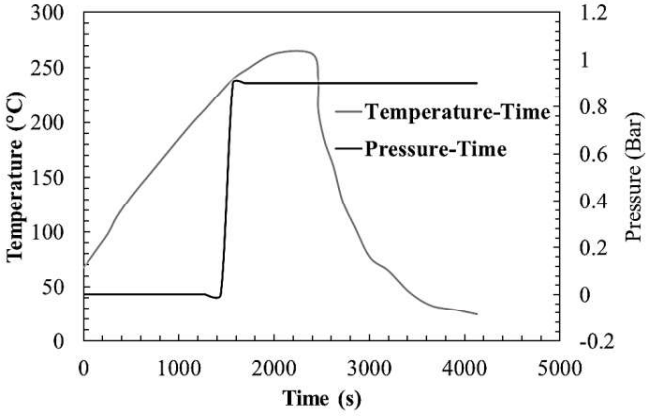
Temperature (°C)
Pressure (Bar)
Time (s)
Temperature-Time
Pressure-Time
300
250
200
150
100
50
0
1.2
1
0.8
0.6
0.4
0.2
0
-0.2
0
1000
2000
3000
4000
5000

(b)

Figure(s)

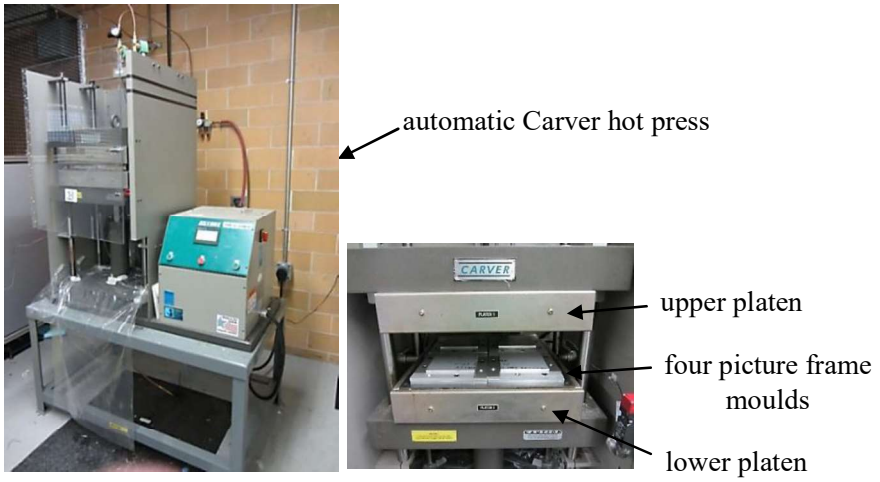
automatic Carver hot press
CARVER
upper platen
four picture frame moulds
lower platen

(a)

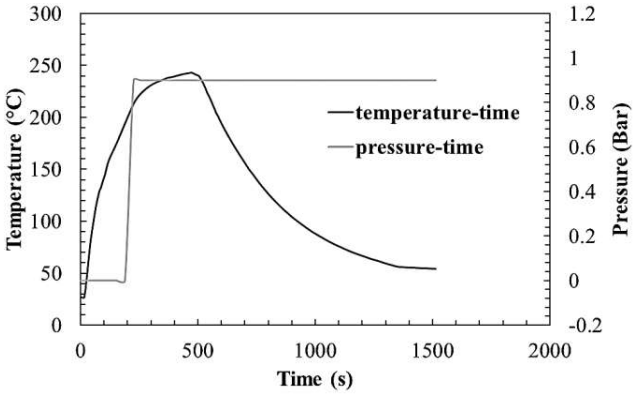
300
250
200
150
100
50
0
Temperature (°C)
1.2
1
0.8
0.6
0.4
0.2
0
-0.2
Pressure (Bar)
temperature-time
pressure-time
0
500
1000
1500
2000
Time (s)

(b)

Figure(s)

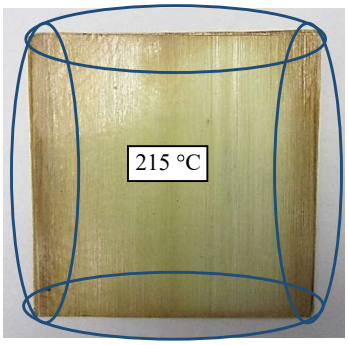

215 °C with 7 minutes dwell time

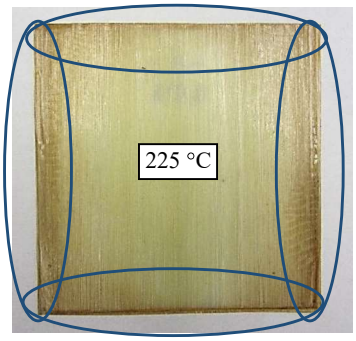

225 °C with 7 minutes dwell time

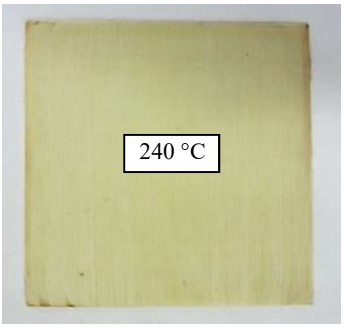

240°C without dwell time

Figure(s)

Process-A

(a

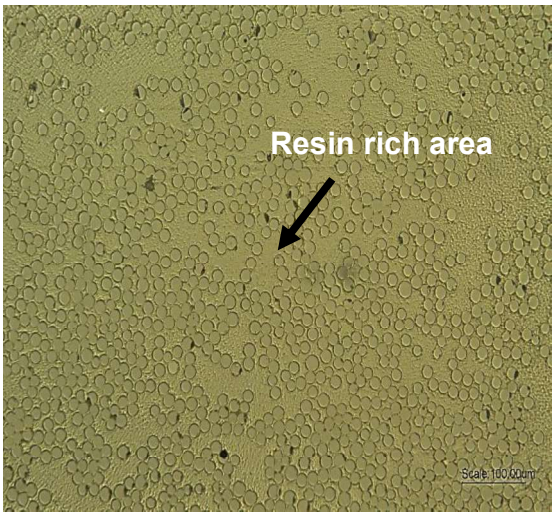

Process-B

(b

Figure(s)

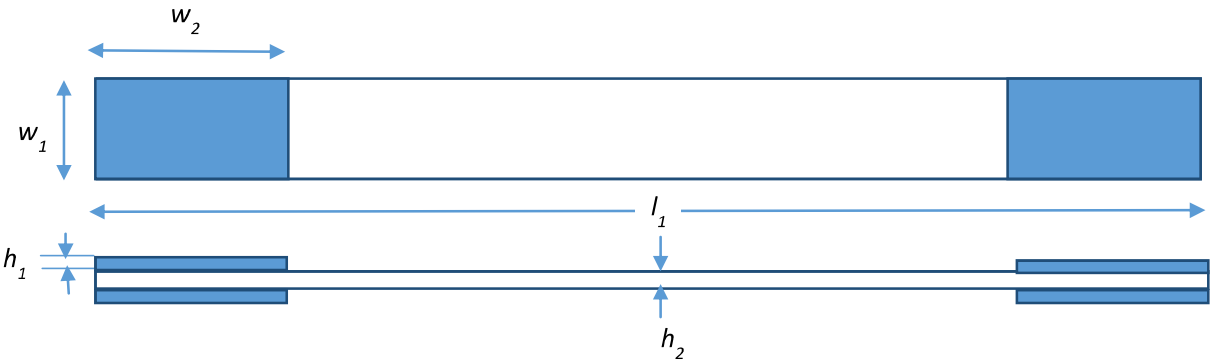

Figure(s)

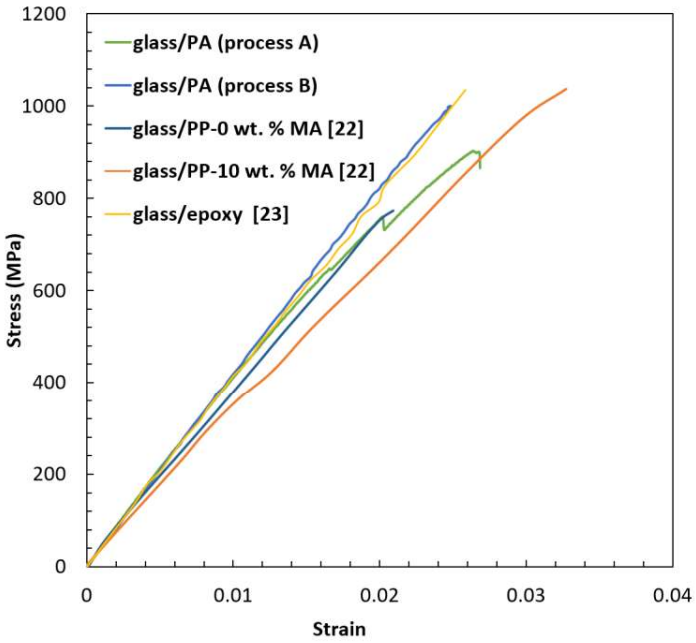
glass/PA (process A)
glass/PA (process B)
glass/PP-0 wt. % MA [22]
glass/PP-10 wt. % MA [22]
glass/epoxy [23]
Stress (MPa)
Strain
0
200
400
600
800
1000
1200
0
0.01
0.02
0.03
0.04

Figure(s)

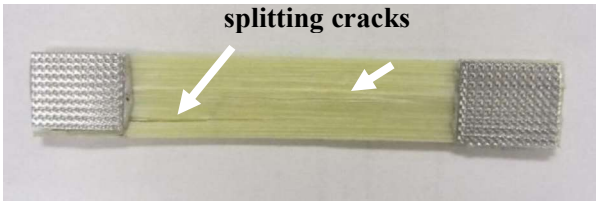

(a)

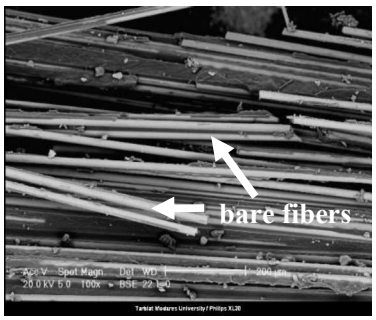

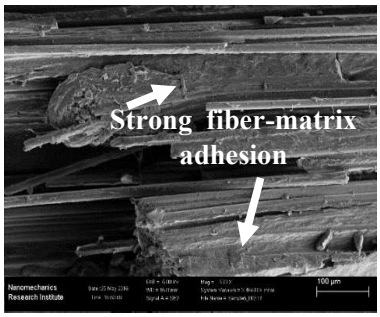

Process-A Process-B

(b)

Figure(s)

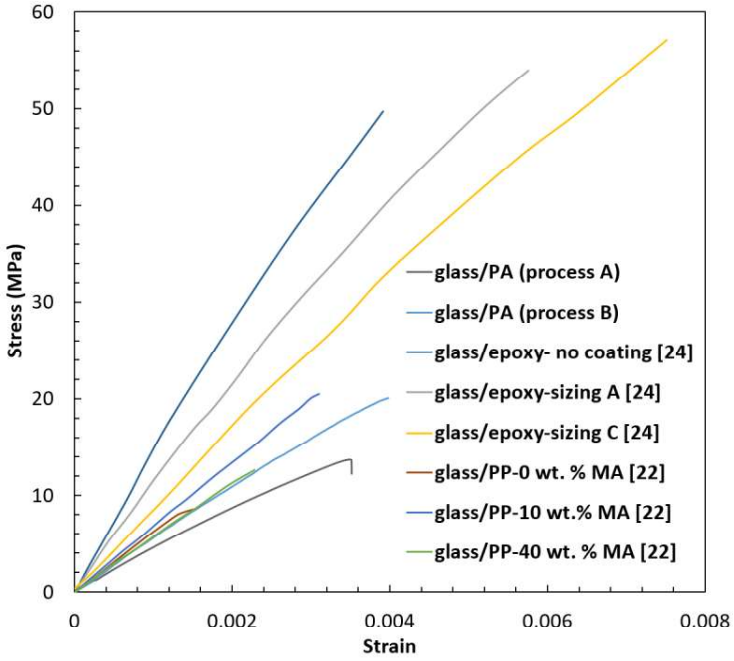
60
50
40
30
20
10
0
Stress (MPa)
0
0.002
0.004
0.006
0.008
Strain
glass/PA (process A)
glass/PA (process B)
glass/epoxy- no coating [24]
glass/epoxy-sizing A [24]
glass/epoxy-sizing C [24]
glass/PP-0 wt. % MA [22]
glass/PP-10 wt.% MA [22]
glass/PP-40 wt. % MA [22]

Figure(s)

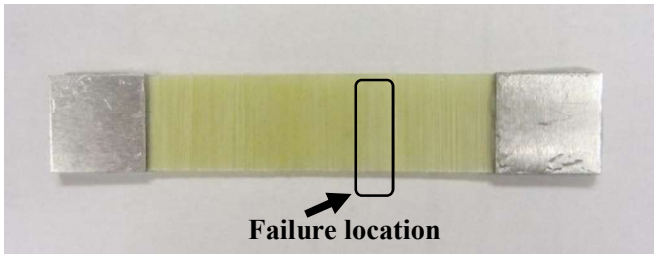

(a)

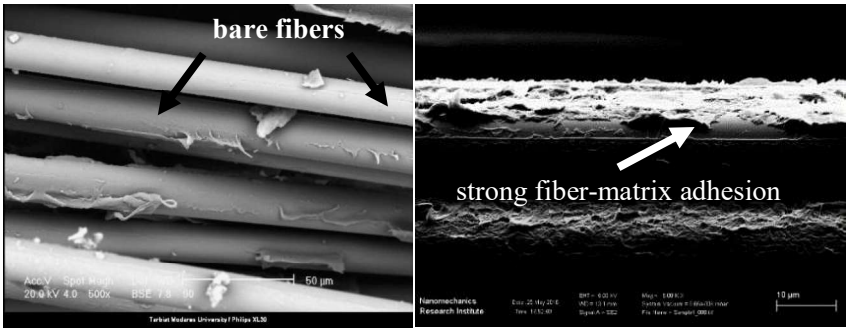

Process-A Process-B

(b)

Figure(s)

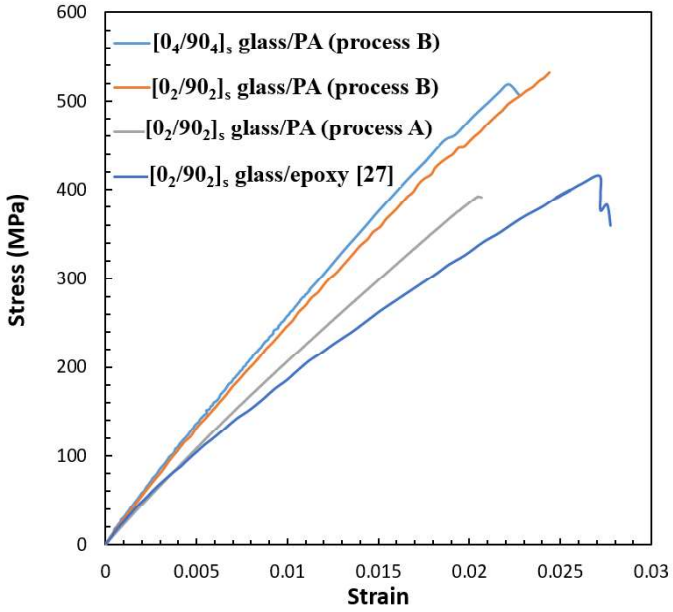
600
500
400
300
200
100
0
Stress (MPa)
0
0.005
0.01
0.015
0.02
0.025
0.03
Strain
[0₄/90₄]s glass/PA (process B)
[0₂/90₂]s glass/PA (process B)
[0₂/90₂]s glass/PA (process A)
[0₂/90₂]s glass/epoxy [27]

Figure(s)

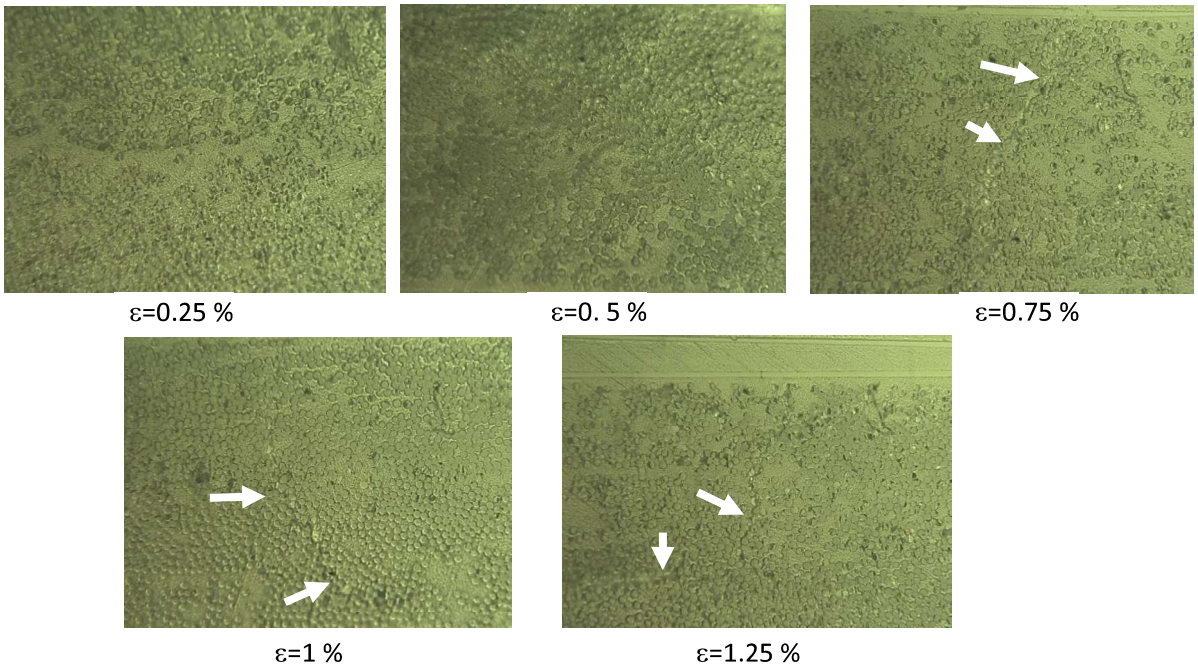

Figure(s)

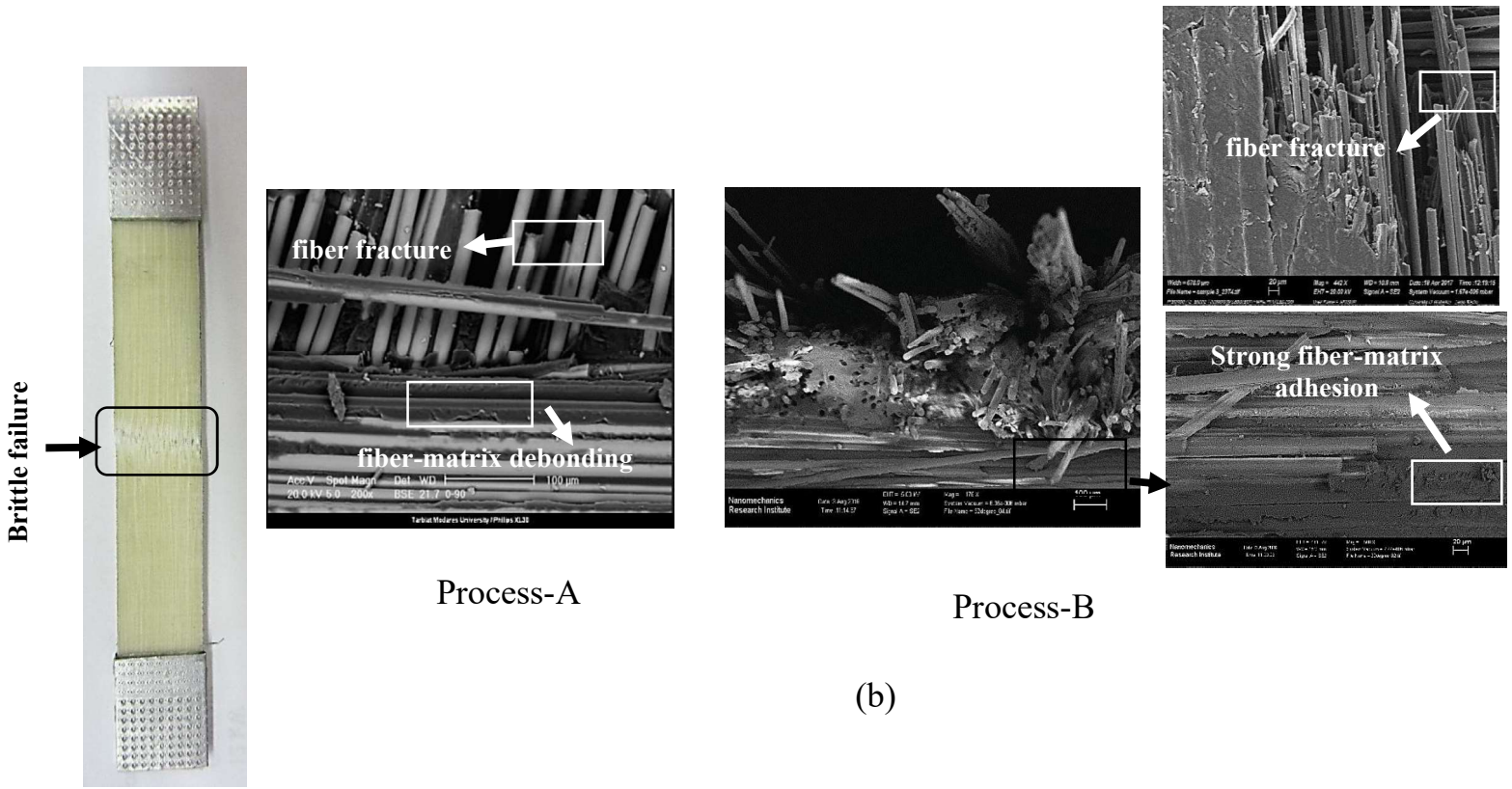
Brittle failure
fiber fracture
fiber-matrix debonding
fiber fracture
Strong fiber-matrix adhesion
Process-A
Process-B
(a)
(b)

Figure(s)

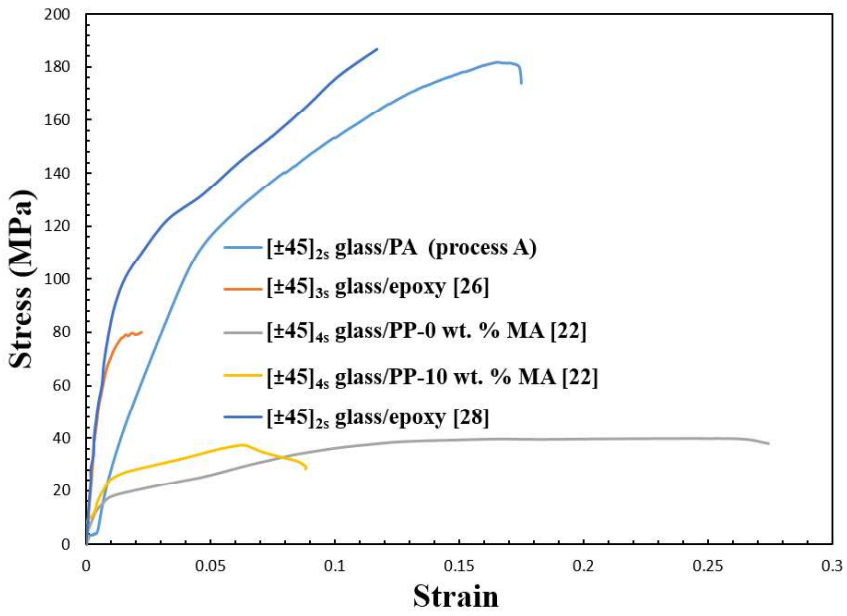
Stress (MPa)
Strain
0
20
40
60
80
100
120
140
160
180
200
0
0.05
0.1
0.15
0.2
0.25
0.3
[±45]2s glass/PA (process A)
[±45]3s glass/epoxy [26]
[±45]4s glass/PP-0 wt. % MA [22]
[±45]4s glass/PP-10 wt. % MA [22]
[±45]2s glass/epoxy [28]